Optimisation of toroidal ZTA anvils and gaskets; towards improved load and pressure performance

N. P. Funnell, C. L. Bull and C. J. Ridley

Published version information

Citation: NP Funnell, CL Bull and CJ Ridley. 'Optimisation of toroidal ZTA anvils and gaskets; towards improved load and pressure performance.' Int J High Pressure Res (2021).

DOI: 10.1080/08957959.2021.1971214

Optimisation of toroidal ZTA anvils and gaskets; towards improved load and pressure performance

N. P. Funnell[a], C. L. Bull[a,b] and C. J. Ridley[a]

[a]ISIS Neutron and Muon Facility, Rutherford Appleton Laboratory, Didcot, OX11 0QX, UK
[b]School of Chemistry, University of Edinburgh, David Brewster Road, Edinburgh, EH9 3FJ, UK

ARTICLE HISTORY
Compiled August 18, 2021

ABSTRACT
We have modified zirconia-toughened alumina anvil geometry and systematically varied single-toroidal, encapsulated, Ti–Zr gasket dimensions, exploring the resulting effects on pressure and maximum load performance, which have been measured using a Paris–Edinburgh press. Reducing the curvature and depth of the recess at the rear of the anvil appears to permit repeated use of the anvils to higher loads, and a general trend indicates that thinner Ti–Zr gaskets may achieve higher pressures than thicker alternatives.

KEYWORDS
Paris–Edinburgh press, neutrons, anvil, gasket

Abbreviations: ZTA: zirconia-toughened alumina, SD: sintered diamond, WC: tungsten carbide, PE: Paris–Edinburgh, ST: single toroid, DT: double toroid

1. Introduction

The Paris–Edinburgh (PE) press [1] has been used with great success to compress a broad range of materials, particularly at neutron facilities worldwide [2–7]. Given the high efficiency of the PE press, there are continued efforts to optimise its performance, expanding the accessible pressure regime, while maintaining data quality [8–11]. The PE press is a load frame that can accommodate a range of anvil types—optimisation often concerns modifications to the geometry of these anvils, or changing the material from which they are made. However, there are stringent restrictions—namely that the anvil should have suitable strength characteristics to withstand significant applied load as well as the large pressures that are generated as a result of this. If the press is used in a 'through-anvil' geometry—where the neutron beam is coincident with the thrust axis, passing through one of the anvils to reach the sample gasket, before being scattered towards detectors arranged perpendicular to the beam direction—it is highly-desirable that the anvils (and gaskets) have favourable neutronic properties.

With respect to reduced attenuation of the neutron beam, the highest quality data are obtained using zirconia-toughened alumina (ZTA, Al_2O_3–ZrO_2) anvils [12], owing

CONTACT N. P. Funnell. Email: nick.funnell@stfc.ac.uk

to their relatively-high transparency to neutrons; a property that is found across a wide range of wavelengths. As a result, these anvils have been used in an increasingly large proportion of high pressure neutron experiments, since their first use at the ISIS Neutron and Muon Facility in 2011 [13,14]. The anvils discussed in this manuscript have a 'Los Alamos' profile [15], where a Bridgman-style cup is combined with an outer-toroid supporting ring [16,17]. Additional support is provided to the anvil when it is press-fitted into a hardened steel fret, which typically uses a 7° bevel angle, matching the incline on the anvil face. These are frequently used in conjunction with a null-scattering 67.6 mol% titanium–32.4 mol% zirconium (Ti–Zr) alloy gasket that encapsulates the sample [18]. With this setup, in our experience on the PEARL instrument [19] at ISIS, the anvils are typically able to endure around 65 tonnes of applied hydraulic load before failure, which usually limits the greatest attainable pressure to ca. 5.5–6.0 GPa. Higher pressures can be obtained straightforwardly using tougher anvils e.g. tungsten carbide (WC) or sintered diamond (SD), which can survive higher applied hydraulic load, but at the expense of reduced neutron transmission which necessitates significantly longer measurement times. Clearly, it would be advantageous to improve on the pressure–load performance of the PE press, while equipped with ZTA anvils.

Any improvement necessitates modifications to the anvil and gasket geometry; indeed, recent works have focussed on modifying the anvil profile and central cup volume in order to maximise the attainable pressure [9,10]. However, the primary obstacles to design improvement are i) the cost/timescales of manufacturing new components—particularly where the effect of minor, systematic changes in dimensions is being explored (though finite element analysis calculations are useful here [8])—and ii) testing the modified components. For the latter point, repeated measurements are required to determine whether observed performance is an exception or the rule but, when this requires costly neutron beamtime, it is usually not possible to carry out testing in significant quantities. Thus it is important to report data from all tests, so that the high pressure community can both build on these findings but also avoid needlessly wasting valuable neutron (or X-ray) beamtime trialling known failed designs, given the time-consuming nature of this process. It is with this intention that herein we detail modifications we have made to anvil and gasket designs, and report the resulting pressure–load performances.

2. Experimental

All modified anvils were first pressed into a hardened steel fret, in an identical manner to standard anvils. In all tests where modifications were made to ZTA anvil geometry (purchased from CeramTec), these were used in conjunction with standard encapsulated Ti–Zr gaskets [18]. Equivalently, when dimensions of the gasket were varied, these were paired with standard 'Los Alamos'-profiled anvils—ZTA, WC, and SD materials were all used over the course of the tests. Figure 1 shows the modified regions of each component; a full list of dimensions is available in the Appendix. Table 1 gives the full list of gasket dimensions trialled, as well as assigning a reference code to each.

In all cases, D_2O was used as a sample (a rationale for this is provided in later discussion) with a coiled piece of lead to act as a pressure marker. The gasket was placed between toroidal anvils in a V3 PE press, and loaded into the PEARL instrument [1,19]. Pressure was increased/decreased via applied oil load, controlled by an automated system. At each load increment, data of sufficient quality to determine the

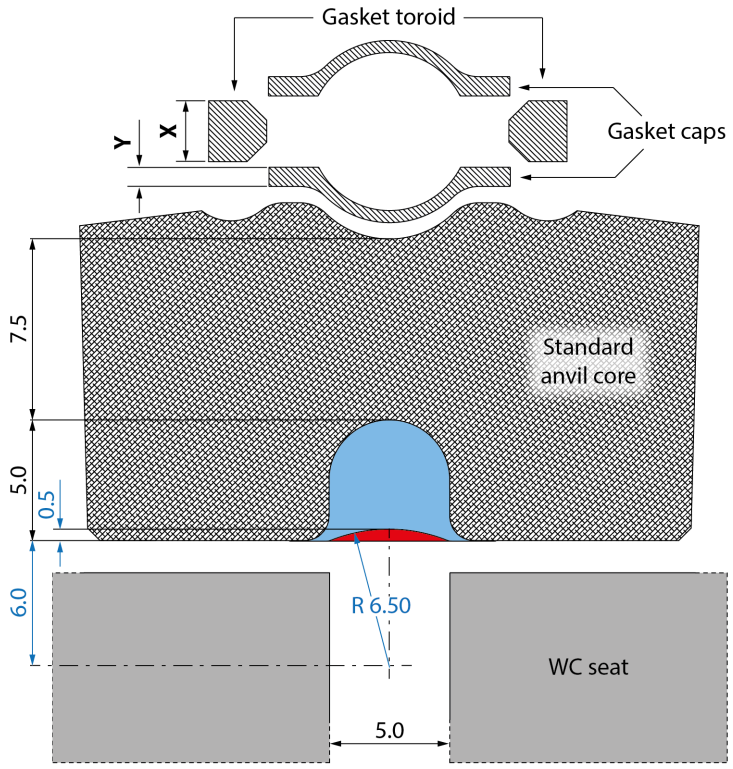

Figure 1. Exploded schematic of the gasket–anvil–seat assembly. The toroid thickness and cap thickness are denoted as 'X' and 'Y', respectively; the trialled dimensions of these are given in Table 1. Modifications made to the standard anvil design are shown in blue for the shallow-recess anvil, and in red where the recess is removed entirely. The WC seat is only partially shown—its inclusion makes clear the positional relationship between its 5 mm beam aperture and the back of the anvil. All dimensions are given in mm. A more comprehensive set of dimensions is available in the Appendix.

pressure unambiguously were obtained. The time-of-flight diffraction data were normalised, and corrected for attenuation by the anvils, using Mantid [20]. Refinements were carried out using Topas 6.0 [21], treating the ice phases with Pawley fits, to avoid any issues with preferred orientation; the anvil components and lead structures were refined with the Rietveld method. Pressure was determined from a 3rd-order Birch-Murnaghan equation of state for lead [22].

3. Results and Discussion

3.1. Modifications to ZTA anvil geometry

The existing anvil design includes a 5 mm diameter recess cut from the back of the anvil (see Figure 1)—this is a legacy from the WC and SD anvils, where it was desirable to remove as much attenuating anvil material as possible from the path of the beam, when using the PE press in a through-anvil geometry. In our experience, any failure at the back of the anvil usually manifests as cracks around, and within, this recess; finite element analysis calculations suggest this is a region of significant stress when the anvil is compressed [8]. Given the high neutron transmission of the ZTA material, we sought to identify whether the removal of the recess in its entirety would afford the anvil greater toughness. As a preliminary check, prior to investigating pressure

Table 1. Toroidal ring (dimension 'X') and gasket cap ('Y') thickness for group A and B gaskets, prior to compression, given in mm. For group A gaskets, a standard Y dimension of 0.8 mm was used. Each gasket was produced in duplicate—designated 'i' and 'ii'. Actual gasket dimensions varied from drawing dimensions. Where any variability in thickness was identified around the cap/ring circumference, the minimum and maximum dimensions are given. Standard gasket dimensions are given for reference.

Reference code	X (design)	X (actual)	Y (design)	Y (actual)
A1i	2.25	2.24–2.29	0.80	–
A1ii		2.29–2.33	0.80	–
A2i	2.75	2.76–2.81	0.80	–
A2ii		2.75–2.81	0.80	–
A3i	3.00	3.04–3.07	0.80	–
A3ii		3.06–3.11	0.80	–
A4i	3.25	3.16–3.24	0.80	–
A4ii		3.28–3.31	0.80	–
B1i	2.25	2.38	0.72	0.70–0.74
B1ii		2.35–2.43		0.72–0.73
B2i	2.75	2.79–2.80	0.88	0.86–0.92
B2ii		2.82–2.83		0.87–0.89
B3i	3.00	3.07–3.08	0.96	0.93–0.98
B3ii		3.07		0.96-0.98
B4i	3.25	3.34	1.04	1.02–1.07
B4ii		3.24–3.26		1.02–1.05
Standard	2.50	–	0.80	–

performance, we measured the influence of removing the recess on the attenuation of the neutron beam. On measuring a Ni pellet between two sets of anvils—one with the recess, and the other without—we found the difference between the two to be negligible. Powder patterns of these measurements are available in the Appendix.

Non-recessed single-toroidal anvils were tested, reaching 9.76(18) GPa with 107.5 tonnes of applied load, before ruinous anvil failure occurred—Figure 2 shows the plotted pressure performance as a function of applied load. We also tested a non-recessed variant of standard double-toroidal anvils; details are given in the Appendix.

It is highly-desirable that the anvils should demonstrate some reusability and so we compressed/decompressed another batch of single-toroid, non-recessed anvils, to 60 tonnes—the load regime deemed 'safe' for the majority of ZTA anvil loadings on PEARL—for comparison with the standard anvil design. Subsequent inspection of the anvils revealed signs of small radial cracks developing around the centre of the anvil (shown in the Appendix) accompanied by a small, cylindrical, protrusion. We determined this to be due to lack of support from the WC seat, which sits behind the anvil (see Figure 1); the beam aperture in the seat was coincident with the position and diameter of the protruding region on the anvil. To mitigate against this effect, we designed a second batch of anvils where a very shallow 0.5 mm recess was machined into the back of the anvil; its curvature just being sufficient to remove any contact between the back of the anvil and the edge of the WC seat beam aperture. A schematic of the modified anvils is shown in Figure 1 and a full set of dimensions is available in the Appendix.

The shallow-recess anvils were used to compress D_2O, reaching 4.34(2) GPa under 60 tonnes of applied load. Though the pressure performance was unremarkable (attributed to probable under-packing of the gasket), crucially, no damage to the anvils was observed. A series of compression/decompression cycles to 90 tonnes were then carried out on the same set of anvils; two cycles were carried out offline and a third online, with neutrons, where the pressure was determined to be 7.681(12) GPa at the maximum load. Progressive, minor, damage was seen to occur in the form of radial

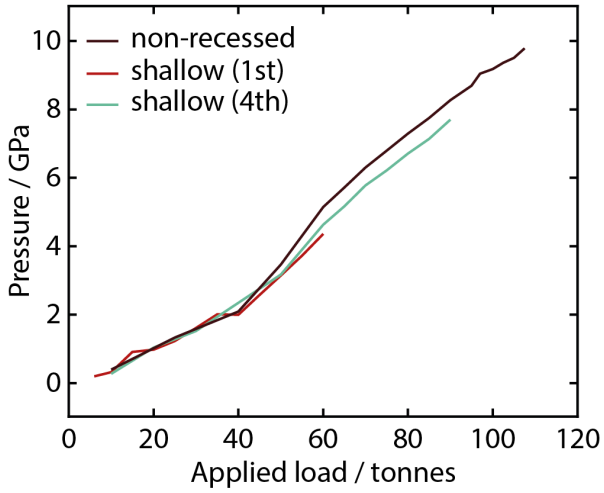

Figure 2. Pressure versus load performance for pairs of non-recessed, and shallow-recess single-toroid ZTA anvils. The '1st' and '4th' labels refer to the specific compression/decompression cycle experienced by the same pair of anvils. Note the second and third cycles were conducted offline; pressures were not determined. The non-recessed anvils failed at the uppermost loads shown here. Error bars on the pressure measurement are omitted for clarity; these do not exceed 0.18 GPa, though they are likely underestimated.

cracking around the recess, but to a far lesser extent than seen for the non-recessed anvils (which failed, entirely, close to this load)—images of the recovered anvils are shown in Figure 3. Only after the third compression to 90 tonnes did more substantial damage occur, in the form of a small chip at the edge of the recess, indicated in the Figure. No damage to the toroidal profile of the anvil face was observed at any stage.

That the anvils withstood a 90 tonne load on repeated pressure increase/decrease (as well as the initial compression to 60 tonnes) is encouraging. For user experiments on PEARL, measurement above ca. 65 tonnes usually necessitates the use of WC or SD anvils, at the expense of both data quality and counting time. Though a few uses of the shallow-recess ZTA to higher loads ultimately resulted in relatively minor anvil damage, the cost of the anvils relative to the extra neutron beamtime that would be required for longer counting with WC and SD, makes the more 'expendable' ZTA an appealing option.

3.2. Modifications to Ti–Zr gasket geometry

From numerous user experiments on the PEARL instrument, the typical performance of a Ti–Zr gasket in single-toroidal ZTA anvils tends to range anywhere between ca. 3.5–6.0 GPa (to a maximum load of ca. 60 tonnes) and we sought to identify how this might be improved upon by modifying the gasket dimensions. Following observations by Bull et al [11] that improved pressure performance resulted when the gasket toroid thickness was increased (with the intention to provide increased radial support when used in anvils with a wider opening angle), we tested two sets of gaskets: i) where the thickness of the outer toroidal ring was varied while keeping the dimensions of the internal caps fixed, and ii) varying the cap and toroidal ring thickness such that a constant ratio between these values was maintained. For brevity, we refer to the first of these as group 'A', and the second 'B'. Within each group, we trialled four different gaskets: three thicker than the standard gasket, used on PEARL, and one thinner.

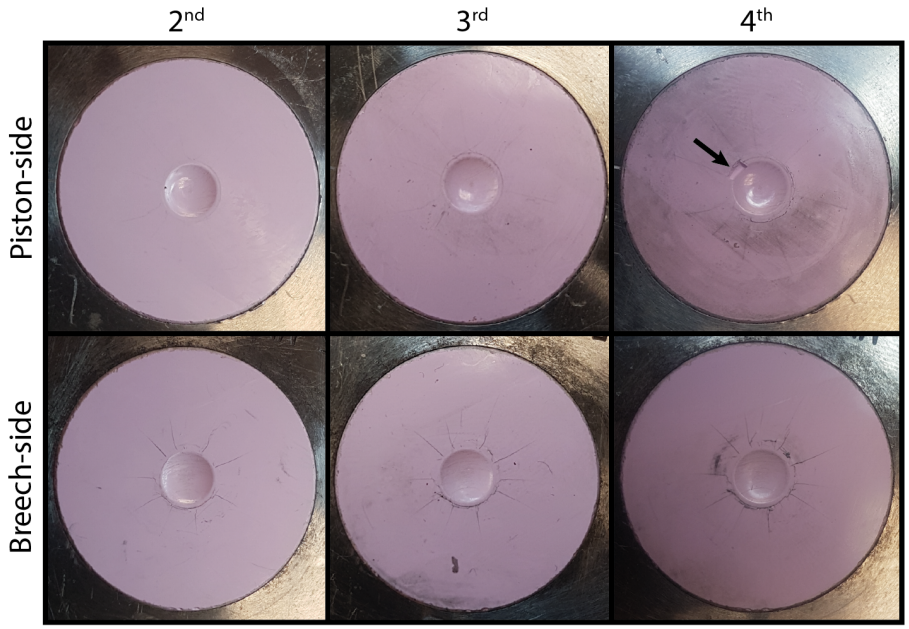

Figure 3. Damage progression in shallow-recess anvils following repeated compression/decompression cycles to 90 tonnes. The majority of the damage to the breech-side anvil is incurred following the second compression. After the fourth compression, a small fragment of the piston-side anvil breaks away, indicated by the arrow in the figure. Note the first compression (not shown here) was performed to 60 tonnes, and no resulting damage was evident.

Figure 1 specifies which dimensions have been varied. Table 1 provides the design, and actual, dimensions of the gaskets (which differ due to machining tolerances), as well as labelling each gasket with a reference code for use with Figure 4.

In any given gasket loading, the maximum attainable pressure is highly-dependent on both the sample packing density and its bulk modulus. Our choice of D_2O as a sample aimed to minimise differences in packing density between each loading as it is easier to completely fill the gasket cups with D_2O than with a powdered sample. Thus the uppermost pressures obtained here are limited by the bulk moduli of liquid D_2O and its high pressure ice phases (VI and VII); the measured pressure might be quite different for a stiffer powdered material. The relative pressures, as a function of gasket dimension, are more important here than the absolute values. In almost all cases oil load was applied up to 60 tonnes (65 tonnes in a couple of instances), in broadly similar increments for all gaskets; any differences are due to time constraints. A plot of the pressure–load performance is presented in Figure 4.

The plotted performances show an approximate indication that thinner gaskets outperform their thicker counterparts—this is seen more clearly in group A than group B. There are a few underperforming gaskets that break this tend, notably A2ii, B1i, and B2i. In these cases, the relatively poor pressures seen here could be ascribed to underpacking of each of the gaskets; obtaining highly-reproducible loadings is still challenging despite our choice of D_2O as a sample. When comparing pressure performance against that of a standard gasket, it is not clear that any of the modified gaskets offer substantially improved behaviour. However, it is reasonably clear that thicker gaskets lead to poorer pressure performance—an observation that may help inform further modifications made during gasket optimisation. We note that the thicker group A gaskets often resulted in severe damage to ZTA anvils; an occurrence not seen with the

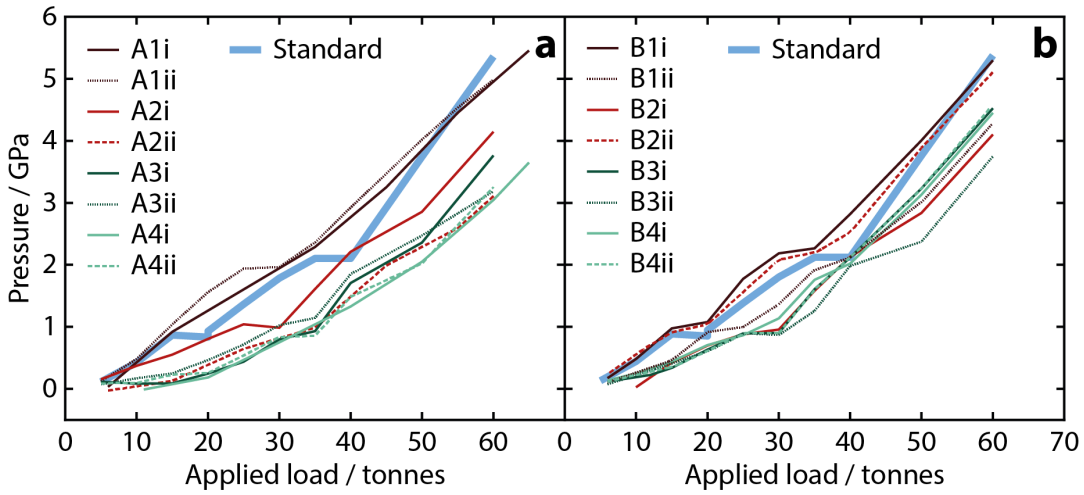

Figure 4. Pressure versus load performance for gaskets from groups A and B. For both groups, the inset legends denotes the gasket reference codes (see Table 1); thickness increases with numbering, ranging between 1–4. An additional plot is included which shows the performance of a standard, unmodified gasket. The abrupt discontinuities seen in each plot can be ascribed to crystallisation of D_2O as ice VI and then subsequent transformation to ice VII. Error bars on the pressure measurement are omitted for clarity; these do not exceed 0.04 GPa, though they are likely underestimated.

group B gaskets. The likely explanation for this is that the reduced dimension complementarity between the toroid ring and inner cap thickness leads to the toroid bearing additional applied load, relative to the central caps. This results in a less smooth pressure distribution across the anvil surface, leading to eventual failure. Following decompression, the gaskets were recovered and their dimensions recorded—these are available in the Appendix.

4. Summary

Modifications to ZTA anvils indicate that the 5 mm recess at the back of the anvil offers minimal neutronic benefit, though its complete removal causes protrusion and radial cracking at the centre of the anvil, when it comes into contact with the aperture in the supporting WC seat at high load. A shallower version of the recess (0.5 mm) with reduced curvature avoids this problem, while allowing repeated use of the anvils to at least 90 tonnes without failure. Further work is required here to establish a more general maximum number of times these shallow-recess anvils can be cycled to high loads and back, though we also note that we find the lifetime of 'standard' ZTA anvils to be quite variable. We have not yet used the shallow recess in conjunction with a double-toroidal profile—this will be investigated in future. A series of gaskets, with systematically varying thicknesses, do not provide a strong indication that changing the thickness provides significant improvement over the standard dimensions. However, an approximate relationship between gasket thickness and attainable pressure has been established, namely that thinner gaskets appear to perform better than their thicker counterparts. These observations may prove useful to the wider pressure community.

Acknowledgements

We thank Colin Offer for assistance in the design process of the anvils and gaskets and we are grateful to the Science and Technology Facilities Council for access to the PEARL instrument.

References

[1] Besson JM, Nelmes RJ, Hamel G, et al. Neutron powder diffraction above 10 GPa. Phys B. 1992;180:907–910.
[2] Iizuka R, Komatsu K, Kagi H, et al. Phase transitions and hydrogen bonding in deuterated calcium hydroxide: High-pressure and high-temperature neutron diffraction measurements. J Solid State Chem. 2014;218:95–102.
[3] Sano-Furukawa A, Hattori T, Komatsu K, et al. Direct observation of symmetrization of hydrogen bond in δ-AlOOH under mantle conditions using neutron diffraction. Sci Rep. 2018;8:15520.
[4] Tulk CA, Molaison JJ, Makhluf AR, et al. Absence of amorphous forms when ice is compressed at low temperature. Nature. 2019;569:542–545.
[5] Terada N, Colin CV, Qureshi N, et al. Pressure-induced incommensurate antiferromagnetic order in a ferromagnetic B-site ordered double-perovskite Lu_2NiMnO_6. Phys Rev B. 2020;102:094412.
[6] Boström HLB, Collings IE, Daisenberger D, et al. Probing the influence of defects, hydration, and composition on Prussian Blue analogues with pressure. J Am Chem Soc. 2021; 143(9):3544–3554.
[7] Salzmann CG, Loveday JS, Rosu-Finsen A, et al. Structure and nature of ice XIX. Nat Commun. 2021;12:3162.
[8] Fang J, Bull CL, Loveday JS, et al. Strength analysis and optimisation of double-toroidal anvils for high-pressure research. Rev Sci Instrum. 2012;83:093902.
[9] Hattori T, Sano-Furukawa A, Machida S, et al. Development of a technique for high pressure neutron diffraction at 40 GPa with a Paris-Edinburgh press. High Pressure Res. 2019;39(3):417–425.
[10] Klotz S, Hansen T, Lelièvre-Berna E, et al. Advances in the use of Paris-Edinburgh presses for high pressure neutron scattering. J Neutron Res. 2019;21:117–124.
[11] Bull CL, Guthrie M, Klotz S, et al. Toroidal anvils for single-crystal neutron studies. High Pressure Res. 2005;25(4):229–233.
[12] Komatsu K, Klotz S, Shinozaki A, et al. Performance of ceramic anvils for high pressure neutron scattering. High Pressure Res. 2014;34:494–499.
[13] Funnell NP, Dawson A, Marshall WG, et al. Destabilisation of hydrogen bonding and the phase stability of aniline at high pressure. CrystEngComm. 2013;15:1047–1060.
[14] Knight KS, Marshall WG, Henderson CMB, et al. Equation of state and a high-pressure structural phase transition in the gillespite-structured phase $Ba_{0.5}Sr_{0.5}CuSi_4O_{10}$. Eur J Mineral. 2013;25(6):909–917.
[15] Klotz S. Techniques in high pressure neutron scattering. Boca Raton (FL): Taylor and Francis; 2013.
[16] Khovstantsev LG. A verkh-niz (up-down) toroid device for generation of high pressure. High Temp High Press. 1984;16:165–169.
[17] Khovstantsev LG, Slesarev VN, Brazhkin VV. Toroid type high-pressure device: history and prospects. High Pressure Res. 2004;24:371–383.
[18] Marshall WG, Francis DJ. Attainment of near-hydrostatic compression conditions using the Paris–Edinburgh cell. J Appl Crystallogr. 2002;35:122–125.
[19] Bull CL, Funnell NP, Tucker MG, et al. PEARL: the high pressure neutron powder diffractometer at ISIS. High Pressure Res. 2016;36(4):493–511.

[20] Arnold O, Bilheux JC, Borreguero JM, et al. Mantid—Data analysis and visualization package for neutron scattering and μSR experiments. Nucl Instrum Meth A. 2014;764:156–166.
[21] Coelho AA. TOPAS and TOPAS-Academic: an optimization program integrating computer algebra and crystallographic objects written in C++. J Appl Crystallogr. 2018; 51(1):210–218.
[22] Fortes AD. A revised equation of state for in situ pressure determination using fcc-Pb ($0 < P < 13$ GPa, $T > 100$ K). STFC; 2019. RAL Technical Reports; RAL-TR-2019-002.

Appendix A. Gasket and anvil dimensions

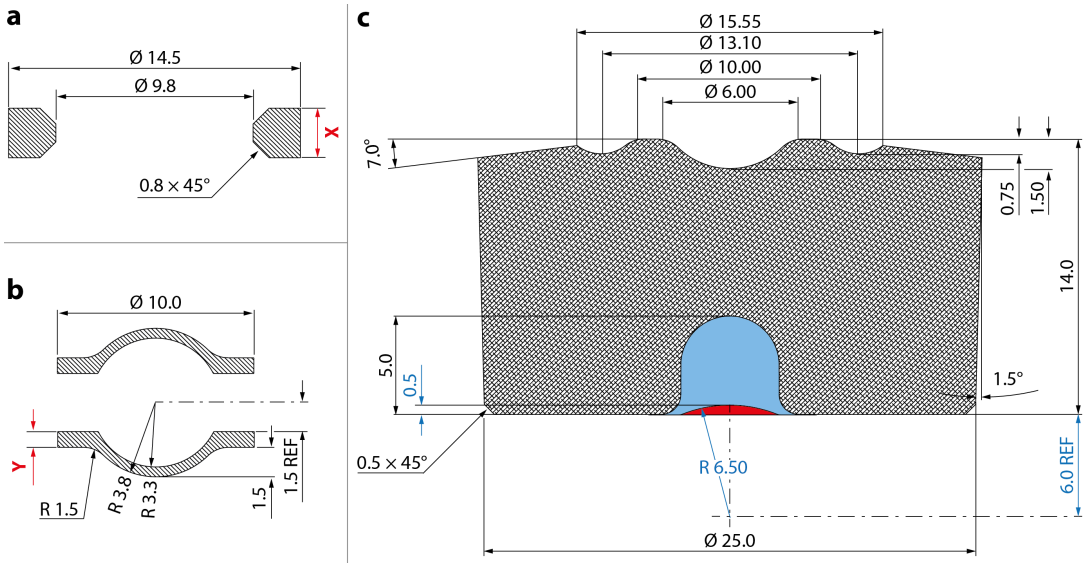

Figure A1. Dimensions used for **a)** outer gasket toroid, **b)** inner gasket caps, and **c)** ZTA anvils. Variable dimensions on the modified gaskets are indicated as 'X' and 'Y'—these are discussed in the main manuscript. Dimensions relating to the shallow-recess anvils are show in blue, and the red region of the anvil indicates the complete removal of the recess. All dimensions are given in mm.

Appendix B. Role of anvil recess on neutron transmission

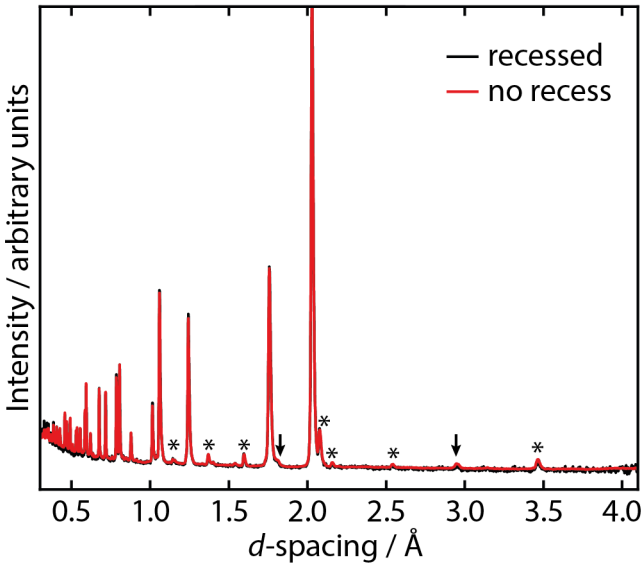

Figure B1. Diffracted neutron signal measured from a Ni pellet between ZTA anvils with (black) a 5 mm recess, and (red) no recess. No attenuation correction has been applied. The negligible difference between the two patterns indicates that filling in the recess does not result in noticeable additional neutron attenuation. Asterisks denote scattering from alumina, and arrows indicate zirconia peaks.

Appendix C. Non-recessed, double-toroidal anvils

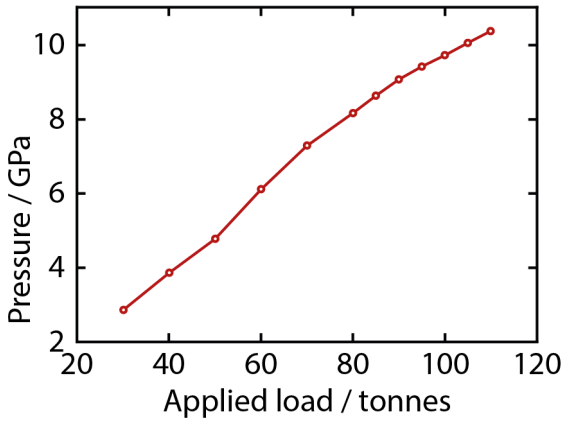

Figure C1. Pressure versus load plot for non-recessed, double-toroidal anvils. Errors are within the size of the data markers. Note that an initial load of 30 tonnes was used. No modifications were made to the anvils beyond removal of the recess; they have a standard double-toroidal profile, and are used with the corresponding double-toroidal encapsulated gaskets. The uppermost load (110 tonnes) produced a pressure of 10.360(9) GPa—the anvils failed, catastrophically, above this load.

Appendix D. Non-recessed, single-toroidal anvils—damage evolution

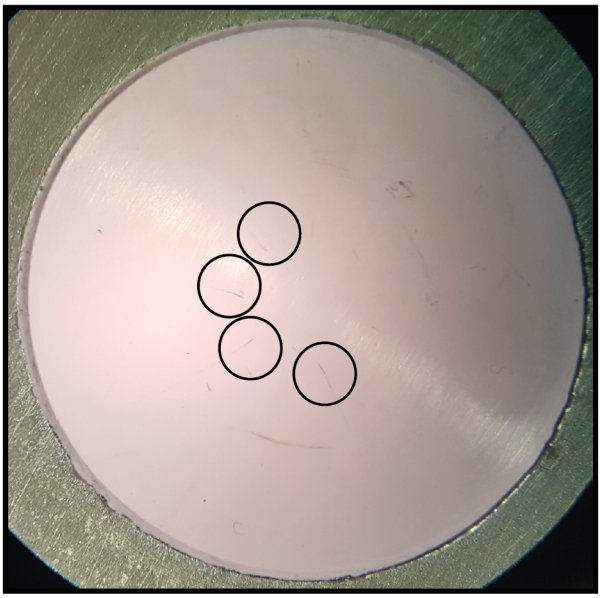

Figure D1. Rear face of non-recessed anvil following 60 tonnes applied load. The formation of small radial cracks is evident, each highlighted by the circled regions. Though not clearly visible in the image, the centre of the anvil has become raised, following its protrusion into the aperture in the WC seat that presses against it.

Appendix E. Post-compression gasket dimensions

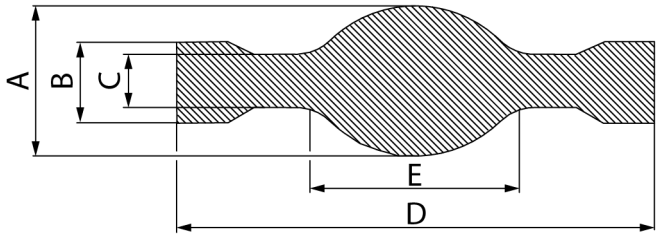

Figure E1. Schematic of sealed gasket, post-compression. Labels 'A–E' indicate the regions measured. Note it is difficult to define the edge of region E—the values determined for this dimension on each gasket are approximate.

Table E1. Post-compression gasket dimensions. The edge of region E is difficult to define, so the values given are approximate. Where multiple regions of the gasket can be sampled, the values are presented as a range, showing the minimum and maximum dimensions found. All dimensions are given in mm. Regrettably, the dimensions of gasket A1ii are unavailable.

Reference code	A	B	C	D	E (approx.)
A1i	4.12	2.11–2.13	0.76–0.79	16.66–16.73	6.44
A1ii	–	–	–	–	–
A2i	4.26	2.24–2.27	1.07–1.16	17.0-17.14	6.41
A2ii	4.15	2.30–2.31	0.91–0.95	16.82–16.94	6.48
A3i	4.31	2.28–2.31	1.08–1.18	17.49–17.69	6.27
A3ii	4.46	2.38–2.40	1.25–1.32	17.18–17.28	6.39
A4i	4.29	2.37–2.38	1.03–1.10	17.60–17.66	6.43
A4ii	4.35	2.34–2.40	1.25–1.27	17.60–17.70	6.31
B1i	4.00	2.21–2.22	0.75–0.78	16.03–16.13	6.26
B1ii	3.98	2.06–2.07	0.68–0.71	16.71–16.84	6.33
B2i	4.20	2.42–2.45	0.96–0.98	16.37–16.41	6.37
B2ii	4.08	2.23–2.24	0.86–0.87	17.42–17.45	6.26
B3i	4.21	2.36–2.38	0.99–1.03	17.46–17.60	6.58
B3ii	4.33	2.27–2.30	1.08–1.12	17.62–17.73	6.16
B4i	4.41	2.58–2.60	1.13–1.18	17.12–17.19	6.58
B4ii	4.29	2.45–2.46	1.10–1.14	17.72–17.80	6.61
Standard	4.17	2.18–2.20	0.92–0.97	17.32–17.63	6.56